ARMY RESEARCH LABORATORY

Performance Bounds on Atmospheric Acoustic Sensor Arrays Operating in a Turbulent Medium II. Spherical-Wave Analysis

Sandra L. Collier and D. Keith Wilson

ARL-TR-2904 **February 2003**

The findings in this report are not to be construed as an official Department of the Army position unless so designated by other authorized documents.

Citation of manufacturer's or trade names does not constitute an official endorsement or approval of the use thereof.

Destroy this report when it is no longer needed. Do not return it to the originator.

Army Research Laboratory

Adelphi, MD 20783-1197

ARL-TR-2904 **February 2003**

Performance Bounds on Atmospheric Acoustic Sensor Arrays Operating in a Turbulent Medium II. Spherical-Wave Analysis

Sandra L. Collier and D. Keith Wilson

Computational and Information Sciences Directorate

Abstract

The performance bounds of a passive acoustic array operating in a turbulent medium with fluctuations described by a von Kármán spectrum are investigated. This treatment considers a single, monochromatic, spherical-wave source and a line-of-sight propagation path. The Cramer-Rao lower bounds of the wave-front angles of arrival are calculated for an unknown parameter set which includes the propagation distance, turbulence parameters, source phase, and signal-to-noise ratio.

Contents

Figures

1. Introduction

The Cramer-Rao lower bounds (CRLBs) of the angle-of-arrival (AOA) estimates for a plane wave incident on a passive sensor array were investigated in Refs. [1,2], herein refered to as the PW Papers. In the PW Papers it was assumed that the wave had propagated through atmospheric turbulence with fluctuations described by a von Kármán spectrum. The received signal was modeled as a complex Gaussian random variable with a non-zero mean. For simplicity, a single monochromatic source and a line-of-sight propagation path were assumed. The technique was based on that of Wilson [3], which followed the general frame work of Song and Ritcey [4].

The present paper is a logical continuation of Refs. [1,2], but for an incident spherical wave. The theoretical model of Refs. [1,2] is used, with the appropriate changes made for a spherical wave. The CRLBs of the azimuthal and elevational AOAs are calculated. The propagation distance, signal-to-noise ratio (SNR), turbulence parameters, and phase of the source are also treated as unknown parameters. As the estimates of the AOAs will degrade when they are simultaneously estimated with other parameters, the couplings between the estimates of the AOAs and the estimates of the other parameters are also calculated.

The paper is ordered as follows: The theoretical model is discussed in section 2 and CRLBs are formulated and discussed in sections 3 and 4. The numerical results and concluding remarks are given in sections 5 and 6, respectively. Tables of the acronyms and symbols are given in appendix A.

2. Theoretical Model

The theoretical model for the probability density function (PDF) of a spherical wave that has propagated through atmospheric turbulence is outlined in this section. The following notation shall be used throughout this paper: $[\cdot]^*$ denotes the complex conjugate, $[\cdot]^{\mathrm{T}}$ the transpose, $[\cdot]^\dagger$ the Hermitian adjoint (complex conjugate transpose), $\langle\cdot\rangle$ the ensemble average or expectation value, and $[\cdot]^\parallel$ and $[\cdot]^\perp$ the vector components parallel and transverse to wave propagation, respectively.

2.1 Signal Model

Consider an array with N sensors. The total received signal at each sensor is taken to be the sum of the wave that has propagated from the source of interest and from noise. Both contributions are time dependent. The total received signal $\mathbf{s}$ may be written as a column vector with N elements, one corresponding to each sensor,

$$\mathbf{s}(\phi,\theta,t) = \mathbf{p}(\phi,\theta,t) + \mathbf{n}(t)\ , \tag{1}$$

where $\mathbf{p}$ is the wave that has propagated from the source with azimuthal and elevational AOAs ϕ and θ, respectively, and where $\mathbf{n}$ is the noise. It is assumed that the noise at the sensors are mutually uncorrelated and that the noise has a complex Gaussian distribution with zero mean and variance σ_n^2 at each sensor. Exact solutions for the pressure field of the source and its PDF are not known, but solutions to its moments are. Therefore, it is approximated that $\mathbf{p}$ is complex Gaussian distributed with mean $\boldsymbol{\mu}$ and covariance matrix $\mathbf{C}_p$,

$$\mu_i = \langle p_i \rangle \quad \text{and} \quad [\mathbf{C}_p]_{ij} = \langle p_i p_j^* \rangle - \mu_i \mu_j^*\ . \tag{2}$$

The moments are determined from the results in the open literature for acoustic wave propagation in a moving random medium as discussed in the following section. We assume that $\mathbf{p}$ and $\mathbf{n}$ are uncorrelated so that the total signal $\mathbf{s}$ is Gaussian distributed with mean $\boldsymbol{\mu}$ and covariance

$$\mathbf{C} = \mathbf{C}_p + \sigma_n^2 \mathbf{I}_N\ . \tag{3}$$

This signal model, in which the real and imaginary parts are Gaussian random variables with equal variances, is reasonable for strong or weak

scattering in the presence of strong diffraction (the Rytov extension region). It is less well suited to situations where both scattering and diffraction are weak (geometric acoustics), in which case the phase variance dominates the signal behavior [8].

2.2 First and Second Moments

The pressure field associated with a sound wave propagating in a moving random medium is characterized by a closed set of fluid dynamic equations. The small-angle parabolic and Markov approximations may be used to obtain the statistical moments of the sound field in closed form. These approximations are valid in far field, for small scattering angles, and for $\mathcal{L} \gg \lambda > \ell$, where λ is the wavelength, and $\mathcal{L}$ and ℓ are the outer (integral) and inner (Kolmogorov) length scales of the turbulence, respectively. We use the solutions for the first and second moments of the pressure field as given by Ostashev [5], who generalized the results in Refs. [6,7] to include fluctuations in the medium velocity. The solution for the second moment is, however, valid for normal incidence across two sensors.

2.2.1 Normal Incidence

Consider a sound wave that is propagating with wave number $\mathbf{k} = k\hat{\mathbf{e}}_r$, $k = 2\pi/\lambda$, where λ is the wavelength of the source. Let the observation point be $\mathbf{r}_i = [x,\ y_i,\ z_i]^{\mathrm{T}}$, so that $x \gg R_i = \left(y_i^2 + z_i^2\right)^{1/2}$. From Ref. [5], the first moment at $\mathbf{r}_i$ for an incident spherical wave is

$$\mu_i = p_{\mathrm{H}}\left(\mathbf{r}_i\right) e^{-\gamma x}\,, \tag{4}$$

where γ is the extinction coefficient for the first moment and p_{H} is the sound field in the absence of random inhomogeneities

$$p_{\mathrm{H}}(\mathbf{r}_i) = p_i\, e^{\mathrm{i}\Phi_i}\,, \quad p_i = \frac{\mathcal{A} r_0}{r_i}\,, \quad \Phi_i = k r_i + \chi\,, \tag{5}$$

where χ is the phase of the source, $\mathcal{A}$ is the pressure at $r_i = r_0$ ($\mathcal{A}$ and r_0 are real-valued constants).

The small-angle approximation (SAA), [i.e., parabolic approximation], for a spherical wave propagating in free space is simply the Taylor series expansion up to first order in $1/x$

$$\frac{\exp\left(\mathrm{i}kr_i\right)}{r_i} \approx \frac{1}{x}\exp\left(\mathrm{i}kx\right)\exp\left(\mathrm{i}\frac{kR_i^2}{2x}\right)\,. \tag{6}$$

Consider now the observation points $\mathbf{r}_i = [x,\ y_i,\ z_i]^{\mathrm{T}}$ and $\mathbf{r}_j = [x,\ y_j,\ z_j]^{\mathrm{T}}$, so that $x \gg R_i,\ R_j$. From Ref. [5], the second moment for normal incidence across sensors i and j is

$$\left\langle p_i p_j^* \right\rangle = p_{\mathrm{H}}\left(\mathbf{r}_i\right) p_{\mathrm{H}}^*\left(\mathbf{r}_j\right)\ e^{-\alpha(\rho_{ij})x}\,, \tag{7}$$

where $\boldsymbol{\rho}_{ij} = \mathbf{r}_i - \mathbf{r}_j$ is the sensor separation vector (transverse to the propagation direction), α is the extinction coefficient for the second moment, and $p_{\mathrm{H}}\left(\mathbf{r}_{i,j}\right)$ are given by the parabolic approximation [equation (6)]. The extinction coefficients for the first and second moments are related by

$$\gamma = \alpha\left(\infty\right)/2\,. \tag{8}$$

2.2.2 Oblique Incidence

We now wish to derive approximate expressions for the first and second moments for oblique incidence. Let the vector from the center of the array to the source be $\mathbf{r} = r\hat{\mathbf{r}}$. The azimuthal and elevational AOAs, ϕ and θ, are measured with respect to the center of the array, so that $\hat{\mathbf{r}} = [\cos\phi\cos\theta,\ \sin\phi\cos\theta,\ \sin\theta]^{\mathrm{T}}$. Let $\mathbf{r}_i' = [x_i',\ y_i',\ z_i']^{\mathrm{T}}$ be the vector from the center of the array to the ith sensor, $\mathbf{r}_i = \mathbf{r} - \mathbf{r}_i'$ be the vector from the ith sensor to the source, and $\boldsymbol{\rho}_{ij} = \mathbf{r}_i - \mathbf{r}_j = \mathbf{r}_j' - \mathbf{r}_i'$ be the vector between the jth and ith sensors. An illustration is given in figure 1. (When comparing results between the plane-wave case and the spherical-wave case, keep in mind that in this paper and in Ref. [2], θ is the elevation, whereas in Ref. [1], θ is the declination and θ' is the elevation.)

For oblique incidence, we must take care in deriving approximations for the moments. A consistent treatment of both the phases and attenuations of the moments is necessary to ensure that the covariance matrix $\mathbf{C}_p$ is non-singular. For normal incidence, the second moment is calculated using the SAA, where $p_{\mathrm{H}}\left(\mathbf{r}_i\right)$ is approximated by expanding about $r_{\|}$ up to first order in $1/r_{\|}$. For oblique incidence, we expand $p_{\mathrm{H}}\left(\mathbf{r}_i\right)$ about r up to first order in $1/r$. In doing so, we assume that the attenuation of the wave across the array is constant and may be approximated by that at the array center. Therefore for $p_{\mathrm{H}}\left(\mathbf{r}_i\right) = p_i \exp\left(\mathrm{i}\Phi_i\right)$, we approximate

$$p_i = \frac{\mathcal{A}r_0}{r_i} \approx \frac{\mathcal{A}r_0}{r} \equiv p_0 \tag{9}$$

$$\Phi_i = \chi + kr_i \approx \chi + k\left[r - \hat{\mathbf{r}}\cdot\mathbf{r}_i' + \frac{r_i'^2 - \left(\hat{\mathbf{r}}\cdot\mathbf{r}_i'\right)^2}{2r}\right]. \tag{10}$$

For the first moment at the ith sensor, we approximate that the attenuation of the wave due to the random medium is also constant across the array

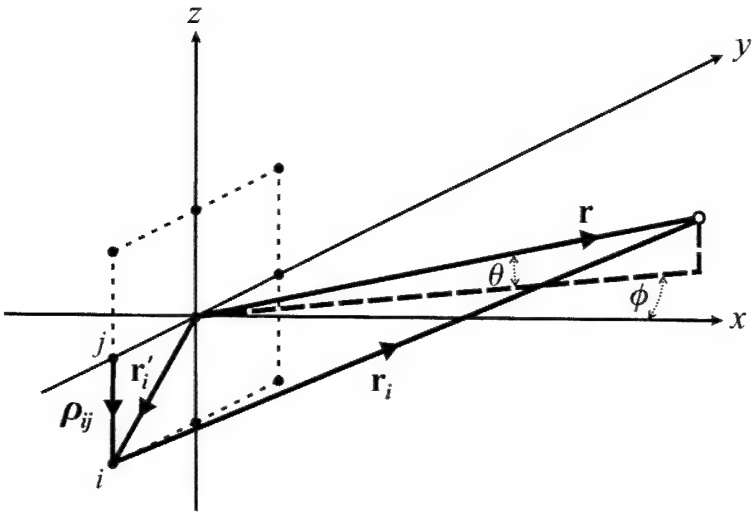

Figure 1. Coordinate system. The closed circles represent the sensors and the open circle represents the source. The azimuth, ϕ, and elevation, θ, are defined with respect to $\hat{\mathbf{r}}$.

and may be approximated by that at the array center. Thus

$$\mu_i \approx p_0 e^{\mathrm{i}\Phi_i} e^{-\gamma r}\,, \tag{11}$$

where Φ_i is given by equation (10).

The second moment for oblique incidence we approximate to be

$$\langle p_i p_j^* \rangle \approx p_0^2 e^{\mathrm{i}\Phi_{ij}} e^{-\alpha(\rho_{ij})\, r} \qquad \Phi_{ij} \equiv \Phi_i - \Phi_j\,, \tag{12}$$

where again Φ_i is given by equation (10). We are thereby assuming that for every i and j,

$$\alpha\big(\rho_{ij}^{\perp}\big) \approx \alpha\big(\rho_{ij}\big)\,. \tag{13}$$

The factor of r in the attenuation term due to the medium is necessary to ensure consistency between the moments. In other words, as

$$[\mathbf{C}_p]_{ij} = \langle p_i p_j^* \rangle - \langle p_i \rangle \langle p_j^* \rangle = p_0^2 \left[e^{-\alpha(\rho_{ij})\, r} - e^{-2\gamma r} \right] e^{\mathrm{i}\Phi_{ij}}\,, \tag{14}$$

in the limit $\rho_{ij} \to \infty$,

$$[\mathbf{C}_p]_{ij} \to p_0^2 \left[e^{-2\gamma r} - e^{-2\gamma r} \right] e^{\mathrm{i}\Phi_{ij}} = 0\,, \tag{15}$$

as it should. Because of these approximations, we limit our investigation to nominally normal incidence at a planar array.

We define the ij-element of the mutual coherence function (MCF) matrix to be the positive square root of

$$\Gamma_{ij}^2 = \frac{\langle p_i p_j^* \rangle \langle p_i^* p_j \rangle}{\langle p_i p_i^* \rangle \langle p_j p_j^* \rangle}\,. \tag{16}$$

For the treatment here,

$$\Gamma_{ij} = |\langle p_i p_j^* \rangle| / p_0^2 = e^{-\alpha(\rho_{ij})\, r}\,. \tag{17}$$

The minimum value of the MCF occuring for $\rho_{ij} = \infty$ is $\Gamma_{\min} = e^{-2\gamma r}$. We define a vector of the phases

$$\boldsymbol{s} = \left[e^{\mathrm{i}\Phi_1},\, e^{\mathrm{i}\Phi_2},\, \cdots,\, e^{\mathrm{i}\Phi_N}\right]^{\mathrm{T}} \tag{18}$$

and the matrix

$$\boldsymbol{\mathcal{S}} = \boldsymbol{s} \otimes \boldsymbol{s}^{\dagger} \tag{19}$$

$$\mathcal{S}_{ij} = \exp\left(\mathrm{i}\Phi_{ij}\right)\,, \tag{20}$$

where $\otimes$ is the (right) Kronecker product. We may then write

$$\boldsymbol{\mu} = p_0 \Gamma_{\min}^{1/2}\, \boldsymbol{s} \tag{21}$$

$$\mathbf{C}_p = p_0^2 \boldsymbol{\Gamma} \odot \boldsymbol{\mathcal{S}} - p_0^2 \Gamma_{\min} \boldsymbol{\mathcal{S}}\,, \tag{22}$$

where $\odot$ is the Hadamard product (element-by-element multiplication). This mathematical expression is useful for computational purposes. As we are approximating that the attenuation of the sound wave is constant across the array, we may think of $\boldsymbol{s}$ and $\boldsymbol{\mathcal{S}}$ as a steering vector and a steering matrix that involve only the phases of the wavefront.

2.3 Turbulence Model

The extinction coefficients depend on the structure of the random medium. For an incident spherical wave the extinction coefficient for the second moment [5,9,10] is

$$\alpha(\rho) = 2\pi k^2 \int_0^1 [f(0) - f(\rho u)]\, du\,, \tag{23}$$

where f is the two-dimensional (2D), or projected, correlation function for the sound speed fluctuations. For most random media, including turbulence, $\alpha\,(\rho)$ initially increases monotonically with increasing ρ, but when ρ exceeds $\mathcal{L}$, $\alpha\,(\rho)$ asymptotically approaches a constant value. Since $f\,(\rho) \to 0$ in the limit $\rho \to \infty$, this constant value is simply 2γ, given by

$$2\gamma = 2\pi k^2 f\,(0) = 2\varsigma^2 k^2 \mathcal{L}\,, \tag{24}$$

where ς^2 is the index of refraction variance. Hence the second moment initially decreases with increasing ρ and eventually "saturates" at a fixed minimum value. Note that this limit [equation (24)] is the same for both an

incident spherical wave [equation (23)] and an incident plane wave [equation (15) of Ref. [1]].

The performance of atmospheric acoustic sensor arrays that have a sensor spacing larger than the height of the array from ground is affected by the large eddies of the energy-containing (or source) subranges of the turbulence spectrum. The isotropic, homogeneous von Kármán turbulence model describes the inertial subrange of the turbulence spectrum more realistically than the commonly used Gaussian models, and it still behaves reasonably in the energy-containing subrange. The von Kármán form for the 2D correlation function is dependent upon the source of the sound speed fluctuations: a scalar field is induced by temperature or humidity fluctuations and a vector field is induced by wind velocity fluctuations. The 2D correlation functions for a scalar field f_s and a vector field f_v, may be written in the form (see equation (49) in Ref. [10] and equation (7.112) in Ref. [5])

$$f_s\left(\rho, \varsigma^2, l\right) = \frac{2\varsigma^2 l}{\sqrt{\pi}\,\Gamma\left(1/3\right)}\left(\frac{\rho}{2l}\right)^{5/6} K_{5/6}\left(\frac{\rho}{l}\right) \tag{25}$$

$$f_v\left(\rho, \varsigma^2, l\right) = \frac{2\varsigma^2 l}{\sqrt{\pi}\,\Gamma\left(1/3\right)}\left(\frac{\rho}{2l}\right)^{5/6}\left[K_{5/6}\left(\frac{\rho}{l}\right) - \frac{\rho}{2l}K_{1/6}\left(\frac{\rho}{l}\right)\right], \tag{26}$$

where $l = \Gamma\left(1/3\right)\mathcal{L}/\left[\sqrt{\pi}\Gamma\left(5/6\right)\right]$ is a characteristic length scale, $\Gamma\left(x\right)$ is the gamma function, and $K_\nu\left(x\right)$ is the modified Bessel function of order ν.

The MCF for an incident spherical wave is plotted in figure 2 as a function of the index-of-refraction variance, ς^2, and the characterstic length scale normalized by the wavelength, l/λ, for both a scalar and a vector von Kármán spectrum. In presenting the results, it is natural to use normalized length scales, (e.g., r/λ, d/λ, etc.), as then the coherence has no explicit wavelength dependence. In (a) and (b) the MCFs are calculated for $\rho/\lambda = 0.5$ and $r/\lambda = 500$. The coherence for both spectra decreases significantly in the regions where the index-of-refraction variance is large, $\varsigma^2 \sim 10^{-4}$, and the normalized characteristic length scale is small, $10 < l/\lambda < 1$. (The MCF is actually dependent upon the product $\varsigma^2 r/\lambda$; therefore, the x-axis alternatively represents an increase in r/λ for fixed ς^2.) In (c) and (d) the same is calculated but for $\rho/\lambda = 3/\sqrt{2}$. The larger sensor separation leads to a more rapid decrease in the MCFs as functions of the turbulence parameters. For both sensor separations the MCF for the vector spectrum is more sensitive to the changes in the turbulence parameters, and its minimum with respect to the turbulence parameters (for a fixed finite sensor separation and normalized propagation distance) is smaller than that for the scalar spectrum.

In order to compare the results to those of the PW Papers, the same has

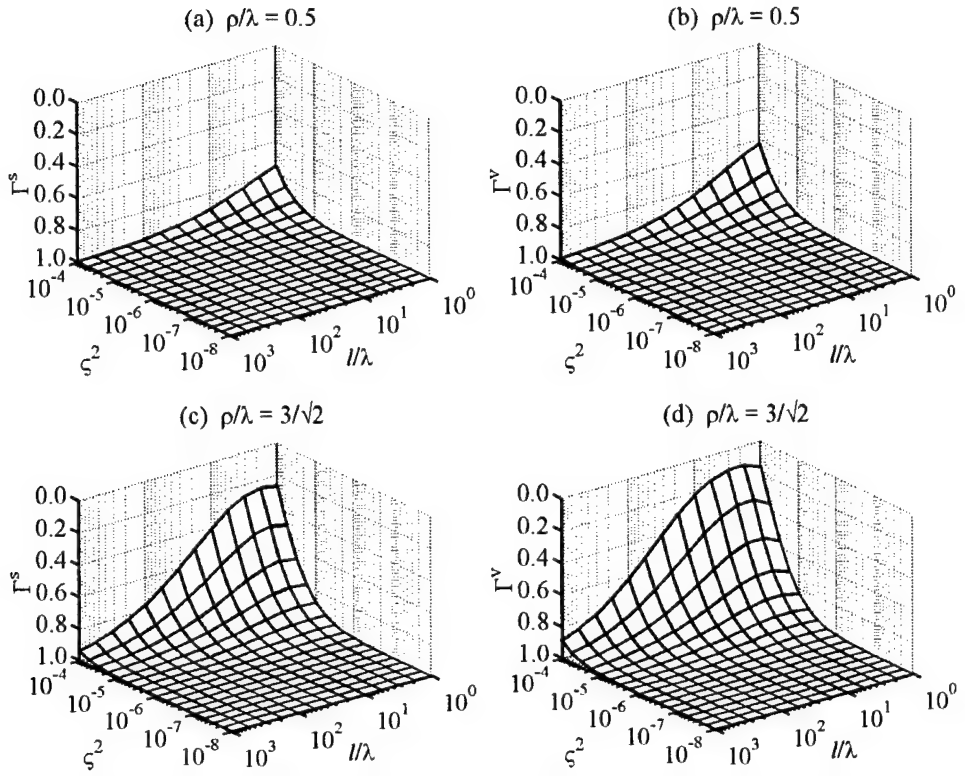

Figure 2. Coherence for an incident spherical wave: (a) and (c) are for a scalar von Kármán spectrum; (b) and (d) are for a vector von Kármán spectrum. All calculations are for $r/\lambda = 500$.

been plotted in figure 3 but for an incident plane wave. Note that the MCF for the spherical wave is larger than that of the corresponding plane wave. Therefore, based on the results from the PW Papers, we expect that the CRLBs of the AOAs for an incident spherical wave should be smaller than those for the corresponding plane wave.

The function $\Gamma_{\min}$ (the minimum value of the MCF as a function of sensor separation ($\rho = \infty$) for fixed propagation distance and fixed turbulence parameters) is the same for both a scalar and a vector spectrum and for both a plane wave and spherical wave. It is plotted in Fig. 4. Even though its value is only dependent upon the product $\varsigma^2 rl/\lambda^2$, it is plotted versus the turbulence parameters at $r/\lambda = 500$ for ease of comparison with figures 2 and 3.

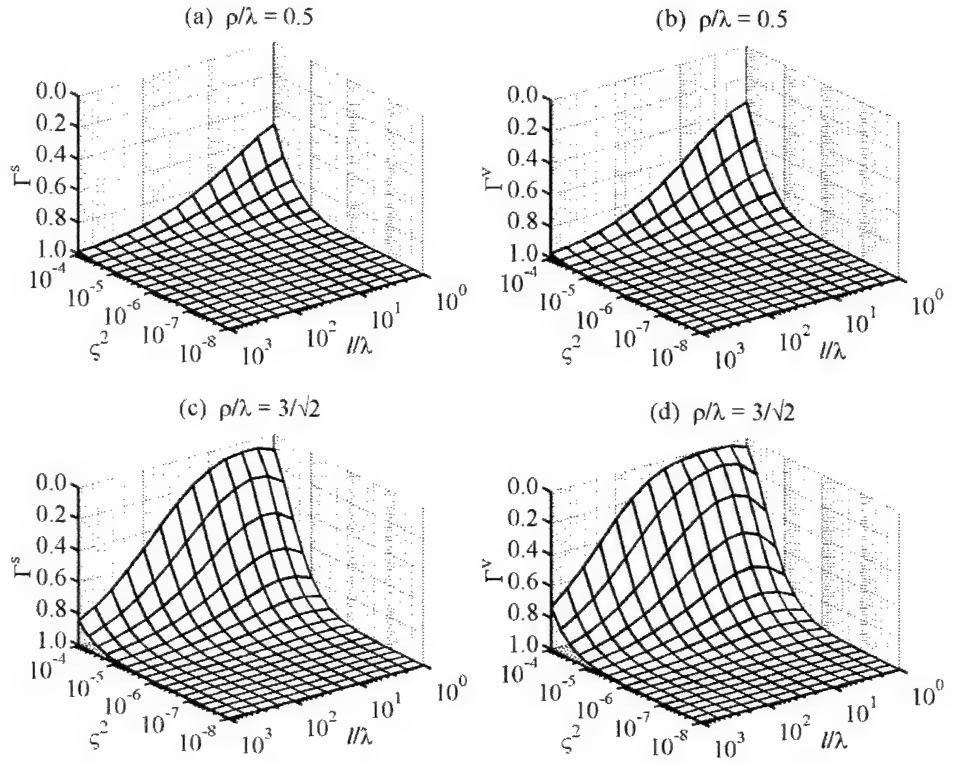

Figure 3. Coherence for an incident plane wave: (a) and (c) are for a scalar von Kármán spectrum; (b) and (d) are for a vector von Kármán spectrum. All calculations are for $r/\lambda = 500$.

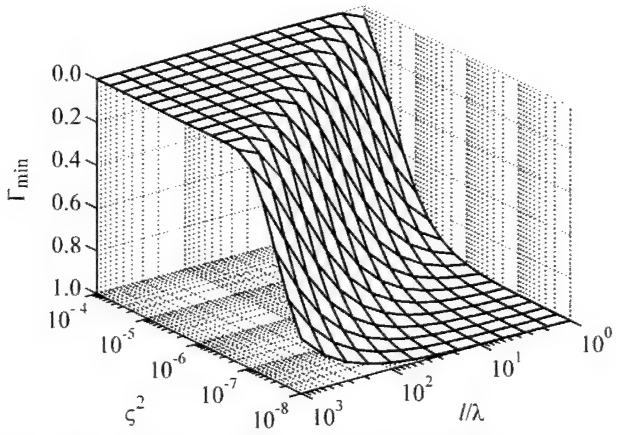

Figure 4. Minimum coherence ($\rho = \infty$) for von Kármán spectra, $\Gamma_{\min} = e^{-2\gamma r}$. Calculation is for $r/\lambda = 500$.

3. Formulation

The CRLB is calculated from the Fisher information (FI), which is dependent upon the PDF. Having completed the theoretical model of the PDF, we now proceed to formulate the FI.

3.1 CRLB

Consider the vector of real parameters $\boldsymbol{\Theta} = [\Theta_1, \Theta_2, \ldots, \Theta_{\mathcal{N}}]^{\mathrm{T}}$ that are to be estimated. The FI for real parameters of a complex Gaussian probability likelihood function with covariance matrix $\mathbf{C}$ and mean $\boldsymbol{\mu}$ is [11]

$$J_{\lambda\nu} = M\mathrm{tr}\left(\mathbf{C}^{-1}\frac{\partial \mathbf{C}}{\partial \Theta_\lambda}\mathbf{C}^{-1}\frac{\partial \mathbf{C}}{\partial \Theta_\nu}\right) + 2M\Re\left(\frac{\partial \boldsymbol{\mu}^\dagger}{\partial \Theta_\lambda}\mathbf{C}^{-1}\frac{\partial \boldsymbol{\mu}}{\partial \Theta_\nu}\right), \tag{27}$$

for M independent and identically distributed data sets. If there are N sensors in the array, $\mathbf{C}$ is an $N \times N$ matrix and $\boldsymbol{\mu}$ is a column vector of length N. Let us use the convention that $\lambda, \nu \in [1, 2, \ldots, \mathcal{N}]$ are the indices on the parameters and $i, j \in [1, 2, \ldots, N]$ are the indices on the sensors.

Let us define $\sigma_\nu = \sqrt{[\mathbf{J}^{-1}]_{\nu\nu}}$. We loosely refer to either σ or σ^2 as the CRLB, as the meaning should be evident from the units involved. The minimum value of σ_ν^2 is $\sigma_{\nu_0}^2 = 1/J_{\nu\nu}$, (i.e., the CRLB when Θ_ν is the only unknown). As the number of unknowns increases, σ_ν^2 will increase.

For example, suppose that there are two unknowns. For λ and ν cyclic (e.g., if $\lambda = 1$ then $\nu = 2$),

$$\sigma_\lambda^2 = \frac{1}{J_{\lambda\lambda} - J_{12}^2/J_{\nu\nu}} = \sigma_{\lambda_0}^2 \frac{1}{1 - \zeta_{12}}, \tag{28}$$

where

$$\zeta_{12} = \frac{J_{12}^2}{J_{11}J_{22}}, \quad 0 \le \zeta_{12} \le 1. \tag{29}$$

Only if $J_{12} = 0$ does $\sigma_\lambda^2 = \sigma_{\lambda_0}^2$, and the estimates of Θ_1 and Θ_2 are said to be uncoupled. As ζ_{12} increases, σ_λ^2 increases from its minimum value of $\sigma_{\lambda_0}^2$, and a degradation of the estimates of Θ_1 and Θ_2 results. The quantity ζ_{12} thus provides a measure of the strength of the coupling between, and hence degradation of, the estimates of Θ_1 and Θ_2: if $\zeta = 0$, the estimates

are uncoupled and the CRLBs retain their minimum values; if $\zeta_{12} \ll 1$, the estimates of θ_1 and θ_2 are weakly coupled and the CRLBs increase only slightly; and if $\zeta_{12} = 1$, the estimates are fully coupled, the CRLBs are infinite, and hence neither Θ_1 nor Θ_2 can be estimated. It is therefore advantageous to determine the conditions under which the estimates of Θ_1 and Θ_2 will decouple.

If there are more than two coupled parameter estimates, we define the coupling between the λth and νth parameter estimates to be

$$\zeta_{\lambda\nu} \equiv \frac{J_{\lambda\nu}^2}{J_{\lambda\lambda} J_{\nu\nu}} \,. \tag{30}$$

In this way, we have a measure of the coupling strength between any two given parameters.

3.2 FI of Theoretical Model

We write the elements of the mean vector as

$$\mu_i = p_0 e^{-\gamma r} e^{\mathrm{i}\Phi_i} = p_0 \Gamma_{\min}^{1/2} e^{\mathrm{i}\Phi_i} \,, \tag{31}$$

and of the total covariance matrix as

$$\begin{aligned} C_{ij} &= p_0^2 \left\{ \left[e^{-\alpha(\rho_{ij})\, r} - e^{-2\gamma r} \right] e^{\mathrm{i}\Phi_{ij}} + \frac{\sigma_n^2}{p_0^2} \delta_{ij} \right\} \\ &= p_0^2 \left[\left(\Gamma_{ij} - \Gamma_{\min} \right) e^{\mathrm{i}\Phi_{ij}} + \frac{\sigma_n^2}{p_0^2} \delta_{ij} \right] \,, \end{aligned} \tag{32}$$

where $\Phi_{ij} = \Phi_i - \Phi_j$ and Φ_i is given by equation (10).

The signal-to-noise ratio is related to the noise variance by $\mathrm{SNR} = p_0^2/\sigma_n^2$. It is often useful to express the SNR in decibels $\mathrm{SNR}_{\mathrm{dB}}$, $\mathrm{SNR} = 10^{\mathrm{SNR}_{\mathrm{dB}}/10}$. For a spherical wave p_0 is dependent upon r; therefore, we consider SNR_0, the signal-to-noise ratio at a distance $\mathcal{R}$, as the unknown. Then $\sigma_n^2 = (\mathcal{A} r_0)^2/(\mathrm{SNR}_0 \mathcal{R}^2)$. By renormalizing the FI by $(\mathcal{A} r_0)^2$, the explicit value of $\mathcal{A} r_0$ is not needed.

The FI may now be readily calculated from equation (27) for those parameters we wish to consider as unknowns: ϕ, θ, χ, r, l, ς^2, and SNR_0. It was shown in the PW Papers that the source phase χ must be treated as an unknown parameter when a non-zero mean is considered; therefore, χ must be treated as an unknown for the spherical-wave case as well. For brevity, the derivatives of the covariance matrix and mean with respect to the unknown parameter set are not presented here.

Due to scale discrepancies between the contributions to the FI matrix, numerical difficulties may arise when trying to invert **J**. As in the PW Papers, we construct a diagonal matrix **D**, whose elements are the inverse of the square-root of the diagonal elements of the FI matrix, $D_{\lambda\nu} = J_{\lambda\nu}^{-1/2}\delta_{\lambda\nu}$. The CRLBs of the unknown parameters may then be determined from

$$\left\langle \left(\Theta_\nu - \hat{\Theta}_\nu\right)^2 \right\rangle = \left[\mathbf{D}\left(\mathbf{DJD}\right)^{-1}\mathbf{D}\right]_{\nu\nu} . \tag{33}$$

The matrix **DJD** may be inverted by standard numerical techniques.

4. Discussion

4.1 No Turbulence

Let us begin by examining the case of no turbulence.

4.1.1 Full SW

In the absence of turbulence, not considering the SAA for the moment,

$$\boldsymbol{\mu} = \left[p_1 e^{\mathrm{i}\Phi_1},\, p_2 e^{\mathrm{i}\Phi_2},\, \ldots,\, p_N e^{\mathrm{i}\Phi_N}\right]^{\mathrm{T}} \quad \text{and} \quad \mathbf{C} = \sigma_n^2 \mathbf{I}_N\,. \tag{34}$$

The elements of the FI matrix are

$$J_{\lambda\nu} = \frac{MN}{\sigma_n^4}\frac{\partial\sigma_n^2}{\partial\Theta_\lambda}\frac{\partial\sigma_n^2}{\partial\Theta_\nu} + \frac{2M}{\sigma_n^2}\sum_{i=1}^{N}\left(p_i^2\frac{\partial\Phi_i}{\partial\Theta_\lambda}\frac{\partial\Phi_i}{\partial\Theta_\nu} + \frac{\partial p_i}{\partial\Theta_\lambda}\frac{\partial p_i}{\partial\Theta_\nu}\right). \tag{35}$$

Suppose that ϕ, θ, and χ are unknown. The elements of the FI are

$$J_{\phi\phi} = \frac{2M}{\sigma_n^2}\sum_{i=1}^{N}\left(\frac{\mathcal{A}^2k^2r_0^2r^2}{r_i^4} + \frac{\mathcal{A}^2r_0^2r^2}{r_i^6}\right)\left[\frac{\partial\left(\hat{\mathbf{r}}\cdot\mathbf{r}_i'\right)}{\partial\phi}\right]^2 \tag{36}$$

$$J_{\theta\theta} = \frac{2M}{\sigma_n^2}\sum_{i=1}^{N}\left(\frac{\mathcal{A}^2k^2r_0^2r^2}{r_i^4} + \frac{\mathcal{A}^2r_0^2r^2}{r_i^6}\right)\left[\frac{\partial\left(\hat{\mathbf{r}}\cdot\mathbf{r}_i'\right)}{\partial\theta}\right]^2 \tag{37}$$

$$J_{\chi\chi} = \frac{2M}{\sigma_n^2}\sum_{i=1}^{N}\frac{\mathcal{A}^2r_0^2}{r_i^2} \tag{38}$$

$$J_{\phi\theta} = \frac{2M}{\sigma_n^2}\sum_{i=1}^{N}\left(\frac{\mathcal{A}^2k^2r_0^2r^2}{r_i^4} + \frac{\mathcal{A}^2r_0^2r^2}{r_i^6}\right)\frac{\partial\left(\hat{\mathbf{r}}\cdot\mathbf{r}_i'\right)}{\partial\phi}\frac{\partial\left(\hat{\mathbf{r}}\cdot\mathbf{r}_i'\right)}{\partial\theta} \tag{39}$$

$$J_{\phi\chi} = -\frac{2M}{\sigma_n^2}\sum_{i=1}^{N}\frac{\mathcal{A}^2kr_0^2r}{r_i^3}\frac{\partial\left(\hat{\mathbf{r}}\cdot\mathbf{r}_i'\right)}{\partial\phi} \tag{40}$$

$$J_{\theta\chi} = -\frac{2M}{\sigma_n^2}\sum_{i=1}^{N}\frac{\mathcal{A}^2kr_0^2r}{r_i^3}\frac{\partial\left(\hat{\mathbf{r}}\cdot\mathbf{r}_i'\right)}{\partial\theta}\,, \tag{41}$$

where

$$\hat{\mathbf{r}} \cdot \mathbf{r}_i' = x_i' \cos\phi \cos\theta + y_i' \sin\phi \cos\theta + z_i' \sin\theta \tag{42}$$

$$\frac{\partial (\hat{\mathbf{r}} \cdot \mathbf{r}_i')}{\partial \phi} = -x_i' \sin\phi \cos\theta + y_i' \cos\phi \cos\theta \tag{43}$$

$$\frac{\partial (\hat{\mathbf{r}} \cdot \mathbf{r}_i')}{\partial \theta} = -x_i' \cos\phi \sin\theta - y_i' \sin\phi \sin\theta + z_i' \cos\theta \,. \tag{44}$$

For the estimates to decouple, the off-diagonal elements must be zero. Substituting equations (42)–(44) into equations (39)–(41) we find

$$J_{\phi\theta} = \frac{2M}{\sigma_n^2} \sum_{i=1}^{N} \left(\frac{\mathcal{A}^2 k^2 r_0^2 r^2}{r_i^4} + \frac{\mathcal{A}^2 r_0^2 r^2}{r_i^6} \right) \Big[\left(x_i'^2 - y_i'^2 \right) \cos\phi \sin\phi \cos\theta \sin\theta$$

$$+ x_i' y_i' \left(\sin^2\phi - \cos^2\phi \right) \cos\theta \sin\theta - x_i' z_i' \sin\phi \cos^2\theta + y_i' z_i' \cos\phi \cos^2\theta \Big] \tag{45}$$

$$J_{\phi\chi} = \frac{2M}{\sigma_n^2} \sum_{i=1}^{N} \frac{\mathcal{A}^2 k r_0^2 r \left(x_i' \sin\phi \cos\theta - y_i' \cos\phi \cos\theta \right)}{r_i^3} \tag{46}$$

$$J_{\theta\chi} = \frac{2M}{\sigma_n^2} \sum_{i=1}^{N} \frac{\mathcal{A}^2 k r_0^2 r \left(x_i' \cos\phi \sin\theta + y_i' \sin\phi \sin\theta - z_i' \cos\theta \right)}{r_i^3} \,. \tag{47}$$

Thus in order for the estimates of ϕ and θ to decouple from the estimate of χ, for every ϕ and θ, we must have

$$\sum_{i=1}^{N} \frac{x_i'}{r_i^3} = \sum_{i=1}^{N} \frac{y_i'}{r_i^3} = \sum_{i=1}^{N} \frac{z_i'}{r_i^3} = 0 \,. \tag{48}$$

Therefore, unlike the PW case, there is no simple array geometry that will result in the decoupling of the estimates of the AOAs from the estimate of the phase angle. The conditions for the estimates of ϕ and θ to decouple are also, in general, unattainable in practice:

$$\sum_{i=1}^{N} x_i'^2 \left(\frac{k^2}{r_i^4} + \frac{1}{r_i^6} \right) = \sum_{i=1}^{N} y_i'^2 \left(\frac{k^2}{r_i^4} + \frac{1}{r_i^6} \right) \tag{49}$$

$$\sum_{i=1}^{N} x_i' y_i' \left(\frac{k^2}{r_i^4} + \frac{1}{r_i^6} \right) = \sum_{i=1}^{N} x_i' z_i' \left(\frac{k^2}{r_i^4} + \frac{1}{r_i^6} \right) = \sum_{i=1}^{N} y_i' z_i' \left(\frac{k^2}{r_i^4} + \frac{1}{r_i^6} \right) = 0 \,. \tag{50}$$

Suppose now that r is also unknown. Then

$$J_{rr} = \frac{2M}{\sigma_n^2} \sum_{i=1}^{N} \left(\frac{\mathcal{A}^2 k^2 r_0^2}{r_i^4} + \frac{\mathcal{A}^2 r_0^2}{r_i^6} \right) \left(r + \hat{\mathbf{r}} \cdot \mathbf{r}_i' \right)^2 \tag{51}$$

$$J_{r\phi} = -\frac{2M}{\sigma_n^2} \sum_{i=1}^{N} \left(\frac{\mathcal{A}^2 k^2 r_0^2 r}{r_i^4} + \frac{\mathcal{A}^2 r_0^2 r}{r_i^6} \right) \left(r + \hat{\mathbf{r}} \cdot \mathbf{r}_i' \right) \frac{\partial \left(\hat{\mathbf{r}} \cdot \mathbf{r}_i' \right)}{\partial \phi} \tag{52}$$

$$J_{r\theta} = -\frac{2M}{\sigma_n^2} \sum_{i=1}^{N} \left(\frac{\mathcal{A}^2 k^2 r_0^2 r}{r_i^4} + \frac{\mathcal{A}^2 r_0^2 r}{r_i^6} \right) \left(r + \hat{\mathbf{r}} \cdot \mathbf{r}_i' \right) \frac{\partial \left(\hat{\mathbf{r}} \cdot \mathbf{r}_i' \right)}{\partial \theta} \tag{53}$$

$$J_{r\chi} = \frac{2M}{\sigma_n^2} \sum_{i=1}^{N} \frac{\mathcal{A}^2 k r_0^2}{r_i^3} \left(r + \hat{\mathbf{r}} \cdot \mathbf{r}_i' \right) . \tag{54}$$

Because of the factor r in the second term in parenthesis, we see that the estimate of r will always be coupled to the estimates of ϕ, θ, and χ, regardless of array geometry.

Also note that none of the elements of the FI given in equations (36)–(41) or (51)–(54) is dependent upon the value of χ. This is expected as the value of the source phase should not effect the estimates of the other parameters. Close inspection of the second term of equation (27) reveals that its dependence in the FI should cancel regardless of whether we consider turbulence or not.

4.1.2 SAA

Let us now consider results for the parabolic approximation using the approximations of p_i and Φ_i given in equations (9) and (10). The elements of the FI matrix are now given simply by

$$J_{\lambda\nu} = \frac{MN}{\sigma_n^4} \frac{\partial \sigma_n^2}{\partial \Theta_\lambda} \frac{\partial \sigma_n^2}{\partial \Theta_\nu} + \frac{2MN}{\sigma_n^2} \frac{\partial p_0}{\partial \Theta_\lambda} \frac{\partial p_0}{\partial \Theta_\nu} + \frac{2Mp_0^2}{\sigma_n^2} \sum_{i=1}^{N} \frac{\partial \Phi_i}{\partial \Theta_\lambda} \frac{\partial \Phi_i}{\partial \Theta_\nu} . \tag{55}$$

We thus find

$$J_{\phi\phi} = \frac{2Mp_0^2 k^2}{\sigma_n^2} \sum_{i=1}^{N} \left[\left(1 + \frac{\hat{\mathbf{r}} \cdot \mathbf{r}_i'}{r} \right) \frac{\partial \left(\hat{\mathbf{r}} \cdot \mathbf{r}_i' \right)}{\partial \phi} \right]^2 \tag{56}$$

$$J_{\theta\theta} = \frac{2Mp_0^2 k^2}{\sigma_n^2} \sum_{i=1}^{N} \left[\left(1 + \frac{\hat{\mathbf{r}} \cdot \mathbf{r}_i'}{r} \right) \frac{\partial \left(\hat{\mathbf{r}} \cdot \mathbf{r}_i' \right)}{\partial \theta} \right]^2 \tag{57}$$

$$J_{\chi\chi} = \frac{2MNp_0^2}{\sigma_n^2} \tag{58}$$

$$J_{rr} = \frac{2MNp_0^2}{\sigma_n^2 r^2} + \frac{2Mp_0^2k^2}{\sigma_n^2}\sum_{i=1}^{N}\left[1 - \frac{r_i'^2 - (\hat{\mathbf{r}}\cdot\mathbf{r}_i')^2}{2r^2}\right]^2 \tag{59}$$

$$J_{\phi\theta} = \frac{2Mp_0^2k^2}{\sigma_n^2}\sum_{i=1}^{N}\left[\left(1 + \frac{\hat{\mathbf{r}}\cdot\mathbf{r}_i'}{r}\right)\frac{\partial(\hat{\mathbf{r}}\cdot\mathbf{r}_i')}{\partial\phi}\right]\left[\left(1 + \frac{\hat{\mathbf{r}}\cdot\mathbf{r}_i'}{r}\right)\frac{\partial(\hat{\mathbf{r}}\cdot\mathbf{r}_i')}{\partial\theta}\right] \tag{60}$$

$$J_{\phi\chi} = \frac{2Mp_0^2k}{\sigma_n^2}\sum_{i=1}^{N}\left[\left(1 + \frac{\hat{\mathbf{r}}\cdot\mathbf{r}_i'}{r}\right)\frac{\partial(\hat{\mathbf{r}}\cdot\mathbf{r}_i')}{\partial\phi}\right] \tag{61}$$

$$J_{\theta\chi} = \frac{2Mp_0^2k}{\sigma_n^2}\sum_{i=1}^{N}\left[\left(1 + \frac{\hat{\mathbf{r}}\cdot\mathbf{r}_i'}{r}\right)\frac{\partial(\hat{\mathbf{r}}\cdot\mathbf{r}_i')}{\partial\theta}\right] \tag{62}$$

$$J_{r\phi} = \frac{2Mp_0^2k^2}{\sigma_n^2}\sum_{i=1}^{N}\left[\left(1 + \frac{\hat{\mathbf{r}}\cdot\mathbf{r}_i'}{r}\right)\frac{\partial(\hat{\mathbf{r}}\cdot\mathbf{r}_i')}{\partial\phi}\right]\left[1 - \frac{r_i'^2 - (\hat{\mathbf{r}}\cdot\mathbf{r}_i')^2}{2r^2}\right] \tag{63}$$

$$J_{r\theta} = \frac{2Mp_0^2k^2}{\sigma_n^2}\sum_{i=1}^{N}\left[\left(1 + \frac{\hat{\mathbf{r}}\cdot\mathbf{r}_i'}{r}\right)\frac{\partial(\hat{\mathbf{r}}\cdot\mathbf{r}_i')}{\partial\theta}\right]\left[1 - \frac{r_i'^2 - (\hat{\mathbf{r}}\cdot\mathbf{r}_i')^2}{2r^2}\right] \tag{64}$$

$$J_{r\chi} = \frac{2Mp_0^2k}{\sigma_n^2}\sum_{i=1}^{N}\left[1 - \frac{r_i'^2 - (\hat{\mathbf{r}}\cdot\mathbf{r}_i')^2}{2r^2}\right]. \tag{65}$$

Notice that the summations on the lowest order terms are the same as those for the PW case [compare to equations (43)–(48) of Ref. [1]]. Therefore, we can use the results from the PW case to minimize the couplings.

Again note that none of the elements of the FI given in equations (56)–(65) is dependent upon the value of χ.

4.2 Turbulence

Let us now consider propagation through atmospheric turbulence.

4.2.1 Two-Element Array

Consider a circular wave that is received at a two-element array. Suppose that the sensors are separated by d. In Appendix D of Ref. [1], the FI is derived for a 2-element array. The results derived there are also valid for the consideration here.

Let $a = C_{11}$, $b = |C_{12}|$, and $c^{1/2} = |\mu_1| = |\mu_2|$, where μ_i and C_{ij} are as defined in equations (31) and (32). As $\partial\Phi_i/\partial\chi = 1\ \forall\ i$, from equation (D-9) of Ref. [1], we know

$$J_{\phi\phi} = \frac{2Mb^2}{a^2-b^2}\left(\frac{\partial\Phi_{12}}{\partial\phi}\right)^2 + \frac{2Mc}{a^2-b^2}\left\{a\left[\left(\frac{\partial\Phi_1}{\partial\phi}\right)^2 + \left(\frac{\partial\Phi_2}{\partial\phi}\right)^2\right] - 2b\frac{\partial\Phi_1}{\partial\phi}\frac{\partial\Phi_2}{\partial\phi}\right\} \tag{66}$$

$$J_{\phi\chi} = \frac{2Mc}{a+b}\left(\frac{\partial\Phi_1}{\partial\phi} + \frac{\partial\Phi_2}{\partial\phi}\right) \tag{67}$$

$$J_{\chi\chi} = \frac{4Mc}{a+b}. \tag{68}$$

If $\partial\Phi_1/\partial\phi = -\partial\Phi_2/\partial\phi$, the estimates of ϕ and χ will decouple for any value of c. The CRLB of ϕ is

$$\sigma_\phi^2 = \frac{1}{J_{\phi\phi} - J_{\phi\chi}^2/J_{\chi\chi}} \tag{69}$$

$$= \frac{a^2-b^2}{M\left[2b^2 + c\,(a+b)\right](\partial\Phi_{12}/\partial\phi)^2}. \tag{70}$$

Now

$$J_{\phi\chi} = \frac{2Mck}{a+b}\left[\left(1+\frac{\hat{\mathbf{r}}\cdot\mathbf{r}_1'}{r}\right)\frac{\partial\left(\hat{\mathbf{r}}\cdot\mathbf{r}_1'\right)}{\partial\phi} + \left(1+\frac{\hat{\mathbf{r}}\cdot\mathbf{r}_2'}{r}\right)\frac{\partial\left(\hat{\mathbf{r}}\cdot\mathbf{r}_2'\right)}{\partial\phi}\right] \tag{71}$$

$$= \frac{2Mck}{a+b}\left[\left(x_1'+x_2'\right)\sin\phi - \left(y_1'+y_2'\right)\cos\phi + \frac{{x_1'}^2 + {x_2'}^2 - {y_1'}^2 - {y_2'}^2}{r}\cos\phi\sin\phi + \frac{x_1'y_1' + x_2'y_2'}{r}\left(\sin^2\phi - \cos^2\phi\right)\right]. \tag{72}$$

In order for $J_{\phi\chi}$ to be zero for every value of ϕ and c, the following must hold

$$0th \text{ order in } 1/r: \qquad x_1' = -x_2' \quad \text{and} \quad y_1' = -y_2' \tag{73}$$

$$1st \text{ order in } 1/r: \qquad {x_1'}^2 + {x_2'}^2 = {y_1'}^2 + {y_2'}^2 \quad \text{and} \quad x_1'y_1' = -x_2'y_2'. \tag{74}$$

The $0th$ order conditions are those found for the PW. However, only one of the two $1st$ order conditions in (74) can hold when (73) holds. Therefore, the estimates of ϕ and χ will always be coupled, but this coupling may be minimized by satisfying equation (73).

If $x_1' = x_2' = 0$ and $y_1' = -y_2' = d/2$, then

$$\left(\frac{\partial \Phi_{12}}{\partial \phi}\right)^2 = k^2 \left[\left(1 + \frac{\hat{\mathbf{r}} \cdot \mathbf{r}_1'}{r}\right) \frac{\partial \left(\hat{\mathbf{r}} \cdot \mathbf{r}_1'\right)}{\partial \phi} - \left(1 + \frac{\hat{\mathbf{r}} \cdot \mathbf{r}_2'}{r}\right) \frac{\partial \left(\hat{\mathbf{r}} \cdot \mathbf{r}_2'\right)}{\partial \phi}\right]^2 = k^2 d^2 \cos^2 \phi \,. \tag{75}$$

Thus

$$J_{\phi\chi} = \frac{Mc^2 k d^2 \cos\phi \sin\phi}{(a+b)\, r} \tag{76}$$

$$= \frac{M\Gamma_{\min}^2 k d^2 \sin 2\phi}{2\left(1 + \Gamma - 2\Gamma_{\min}^2 + \sigma_n^2/p_0^2\right) r} \tag{77}$$

$$= \frac{M e^{-2\gamma r} k d^2 \sin 2\phi}{2\left[1 + e^{-\alpha(d/2)r} - 2e^{-2\gamma r} + \sigma_n^2/p_0^2\right] r} \,. \tag{78}$$

At normal incidence, $\phi = 0$, the coupling is zero. This term decays by at least $e^{-2\gamma r}/r$, therefore at large values of r, $J_{\phi\chi}$ decays very rapidly. It follows that

$$\sigma_\phi^2 = \frac{a^2 - b^2}{M k^2 d^2 \cos^2\phi \left[2b^2 + c\,(a+b)\right]} \tag{79}$$

$$= \frac{1 - \Gamma^2 - 2\Gamma_{\min}\left(1 - \Gamma_{\min}\right) + 2\sigma_n^2/p_0^2\left(1 - \Gamma_{\min}\right)}{M k^2 d^2 \cos^2\phi \left[2\Gamma^2 - 3\Gamma\Gamma_{\min} + \Gamma_{\min}\left(1 + \sigma_n^2/p_0^2\right)\right]} \,. \tag{80}$$

This is the same as found for the PW, except that p_0 now has a $1/r$ dependence. Note that the 1*st* order corrections in the phase term canceled.

4.2.2 Planar Array

For full three-dimensional (3D) propagation in turbulence, we assume that the wave is propagating near the x-axis, take the array plane to be the yz-plane, and take the origin to be at the center of the array. Numerically, we find: the estimates of ϕ, θ, r, and χ are all coupled; the estimates ϕ and θ are uncoupled from the estimates of ℓ, ς^2, and SNR_0; and the estimates of r, ℓ, ς^2, and SNR_0 are all coupled. The results are independent of the value of χ.

5. Results

The array geometry considered for this analysis is a 4×4 square grid with spacing of d. In all figures $d/\lambda = 0.5$. As the CRLB (σ) for M independent and identically distributed datasets is $1/\sqrt{M}$ times the CRLB for one dataset, all results are presented for $M = 1$.

5.1 CRLB of AOAs

As the estimates of the AOAs are only coupled to the esimates of χ, r/λ, ϕ, and θ, only these four parameters are considered as unknowns in this section.

Due to the symmetry of the array, the values of σ_ϕ and σ_θ are the same at normal incidence. At $\phi = 0$, the couplings $\zeta_{\phi\theta}$, $\zeta_{\phi\chi}$, and $\zeta_{\phi r/\lambda}$ are all zero. And at $\theta = 0$, the couplings $\zeta_{\phi\theta}$, $\zeta_{\theta\chi}$, and $\zeta_{\theta r/\lambda}$ are all zero. Therefore, at $\phi = \theta = 0$, $\sigma_\phi = \sigma_\theta = \sigma_{\phi 0} = \sigma_{\theta 0}$. All the angular couplings increase with increasing ϕ and θ.

In figure 5, σ_ϕ for normal incidence is plotted versus ℓ/λ and ς^2 for $r/\lambda = 500$ and $\mathrm{SNR}_0 = 10$ dB at $\mathcal{R}/\lambda = 500$. A scalar von Kármán spectrum is used. The overall values of σ_ϕ are smaller than for the plane-wave case (see figure 16 of Ref. [1] or figure 11 of Ref. [2]). This is expected as the values of the MCF for a plane wave are smaller than for a spherical wave (refer to figures 2–3 on pg. 9). The same is plotted in figure 6, but for a vector von Kármán spectrum. The ratio $\sigma_\phi^v/\sigma_\phi^s$, where the superscripts refer to the type of spectrum, is plotted in figure 7. As expected, σ_ϕ for the vector spectrum is larger than that for the scalar spectrum. As with the PW case, the use of a non-zero mean reduces the CRLBs of the AOAs. For other values of ϕ and θ, the behavior of CRLBs of the AOAs is similiar, with σ_ϕ and σ_θ increasing with increasing ϕ and θ. And for other values of the SNR, the behavior is similar.

In figure 8, σ_ϕ is plotted versus the normalized propagation distance for normal incidence and a scalar von Kármán spectrum. Two values of ς^2, ℓ/λ, and SNR_0 evaluated at $\mathcal{R}/\lambda = 500$ are considered. In order to see the limiting behavior of the model, the graph is extended to include smaller values of r/λ than are valid for the turbulence model. At small values of r/λ, we see that σ_ϕ is dependent upon the values of the turbulence parameters (particularly ς^2) and is independent of the value of SNR_0 (as it

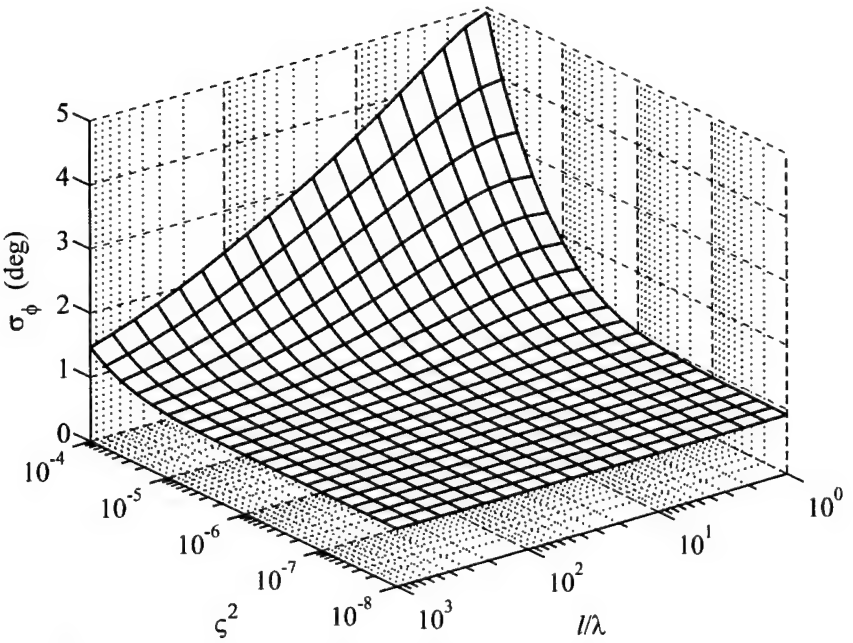

Figure 5. CRLB of azimuth as a function of turbulence parameters for a scalar von Kármán spectrum: normal incidence, $r/\lambda = 500$, and $\mathrm{SNR}_0 = 10$ dB at $R_0/\lambda = 500$. Due to symmetry, $\sigma_\phi = \sigma_\theta = \sigma_{\phi_0} = \sigma_{\theta 0}$ at $\phi = \theta = 0$.

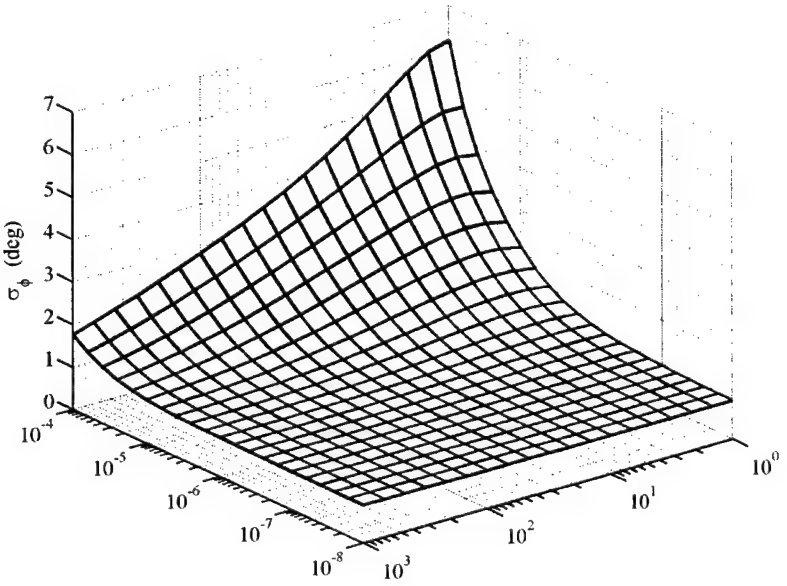

Figure 6. CRLB of azimuth as a function of turbulence parameters for a vector von Kármán spectrum. All other parameters same as figure 5.

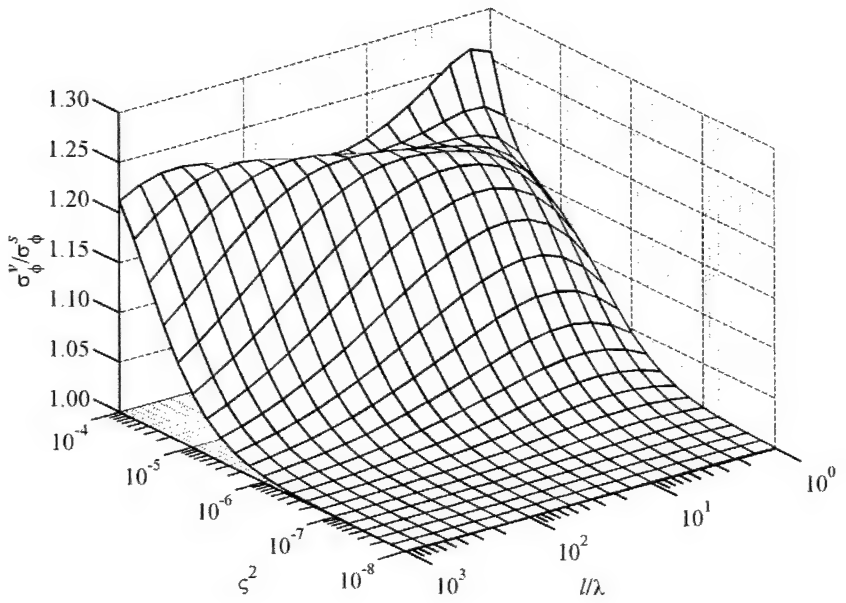

Figure 7. Ratio of σ_ϕ^v to σ_ϕ^s as a function of turbulence parameters. Parameters same as figures 5 and 6.

should be as SNR_0 is evaluated at $\mathcal{R}/\lambda = 500$). Note the difference between the outward spherical wave propagation and the plane wave propagation depicted in figure 18 of Ref. [1] and figure 13 of Ref. [2].

The same is investigated in figure 9 but for $\phi = \theta = 15°$. While σ_ϕ has increased slightly, the behavior is the same. The coupling between ϕ and θ is in figure 10. For $r/\lambda = 10$, $\zeta_{\phi,\theta}$ is dependent upon the values of the SNR and the turbulence parameters; however, this dependence rapidly vanishes and $\zeta_{\phi,\theta}$ becomes constant for $r/\lambda > 100$. Therefore, for values of r/λ that are consistent with the SAA, $\zeta_{\phi,\theta}$ is independent of ς^2, ℓ/λ, and SNR_0. Figure 11 depicts the coupling between ϕ and χ. For all values of ς^2, ℓ/λ, and SNR_0, $\zeta_{\phi,\chi}$ diminishes exponentially with increasing r/λ. The coupling between ϕ and r/λ is plotted in figure 12. Again for large values of r/λ, $\zeta_{\phi,r/\lambda}$ diminishes exponentially. The analogous graphs of figures 9–12 for θ (instead of ϕ) have the same behavior.

The behavior of σ_ϕ and σ_θ, as well as all the couplings, as a function of propagation distance is the same for a vector von Kármán spectrum. The values of σ_ϕ and σ_θ are slightly higher. Refering back to figure 10, the coupling $\zeta_{\phi,\theta}$ for a vector spectrum has similar values for $r/\lambda < 100$ and approaches the same constant for $r/\lambda > 100$.

The angular dependence of the CRLBS of the AOAs are shown in figure 13

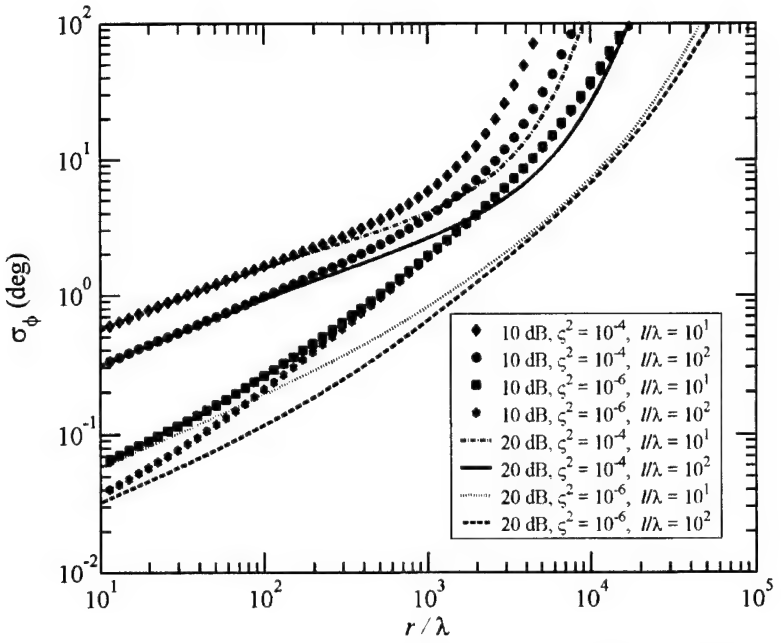

Figure 8. CRLB of azimuth as a function of normalized propagation distance for normal incidence. SNR evaluated at $\mathcal{R}/\lambda = 500$, scalar von Kármán spectrum.

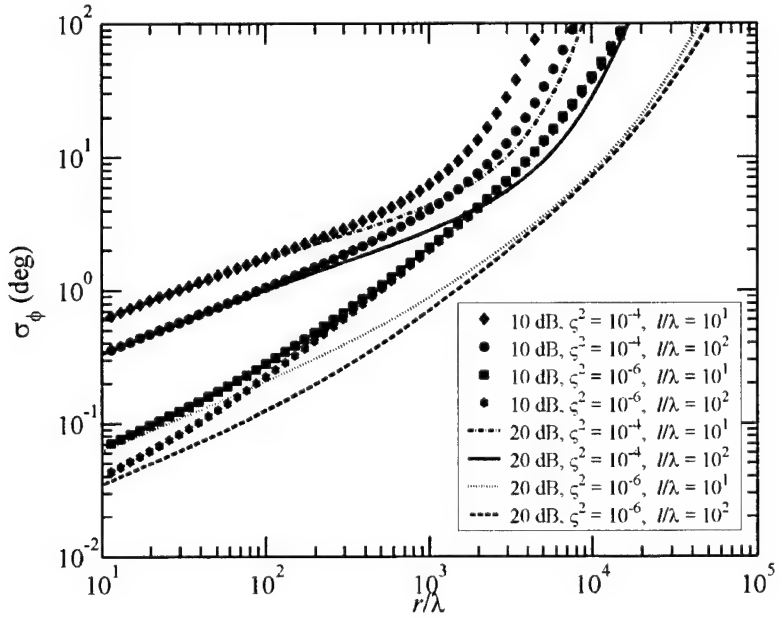

Figure 9. CRLB of azimuth as a function of normalized propagation distance for $\phi = \theta = 15°$. All other parameters same as in figure 8. (Analogous plots for σ_θ have same behavior, though smaller values.)

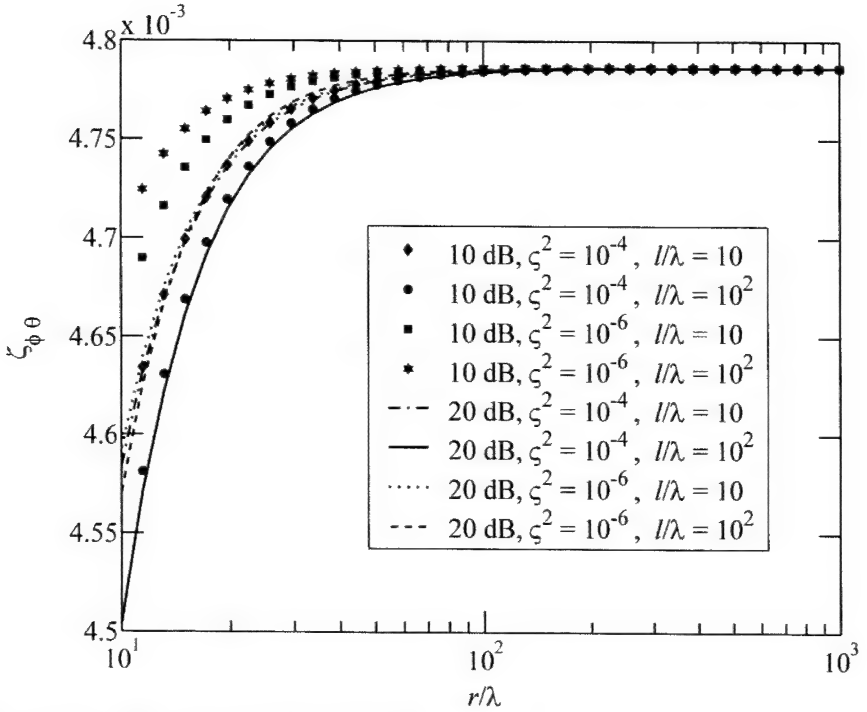

Figure 10. Coupling between ϕ and θ as a function of normalized propagation distance. Parameters same as figure 9.

and the coupling between the AOAs is shown in figure 14 for a scalar von Kármán spectrum. In 13(a–c), $\varsigma^2 = 10^{-4}$, $\ell/\lambda = 10$, $r/\lambda = 500$, and $\mathrm{SNR}_0 = 10$ dB at $\mathcal{R}/\lambda = r/\lambda$. We see the same symmetry in σ_ϕ as in the PW case, and σ_θ is again independent of azimuth. (Refer to figures (15–16) in Ref. [2] and figures (21–22) in Ref. [1].) Not shown are $\zeta_{\phi,r/\lambda}$ and $\zeta_{\theta,r/\lambda}$, which are at most $\sim 10^{-12}$ at $\phi = \theta = 15°$. To within the numerical accuracy of the calculation, $\zeta_{\phi,\chi}$ and $\zeta_{\theta,\chi}$ are both zero. In 13(d–f), all the parameters are the same except $\varsigma^2 = 10^{-6}$. The CRLBs have decreased, as expected. Here $\zeta_{\phi,r/\lambda}$, $\zeta_{\theta,r/\lambda}$, $\zeta_{\phi,\chi}$, $\zeta_{\theta,\chi} \sim 10^{-9}$ at $\phi = \theta = 15°$. The coupling $\zeta_{\phi,\theta}$ in figure 14 is the same for both cases. In fact, the coupling between ϕ and θ is the same (only .02 percent difference) as for the PW case for all parameters and both spectra when $r/\lambda \gtrapprox 100$. The analogous results for a vector spectrum have the same behavior.

It is found for all cases, that the use of a non-zero mean reduces the CRLBs of the AOAs. However, in the regions where the AOAs can be estimated, this percent difference is small, usually less than two percent. This percent difference is discussed in detail in Ref. [12] for both an incident spherical and plane wave.

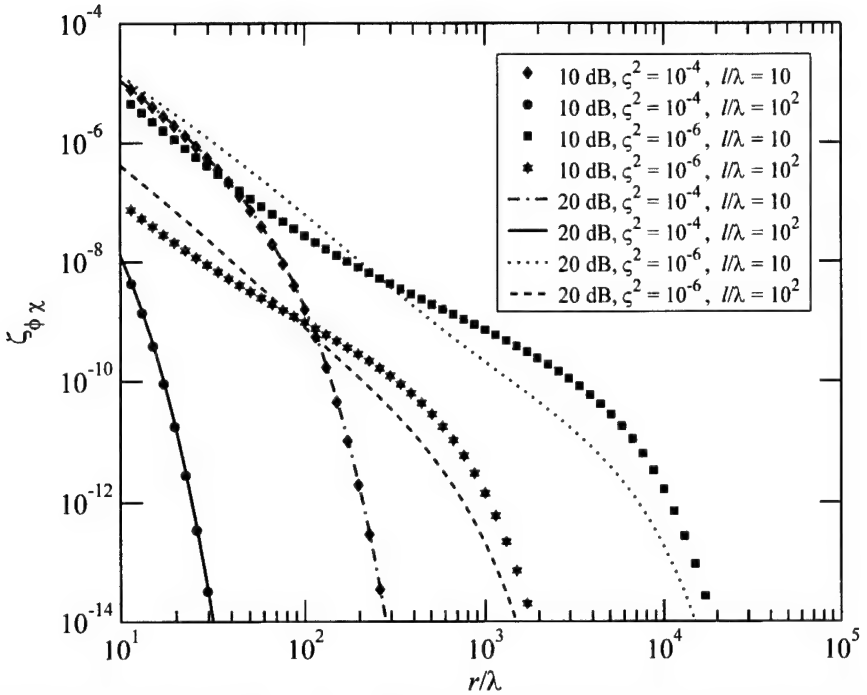

Figure 11. Coupling between ϕ and χ as a function of normalized propagation distance. Parameters same as figure 9. (Analogous plots for $\zeta_{\theta,\chi}$ have same behavior and almost same values.)

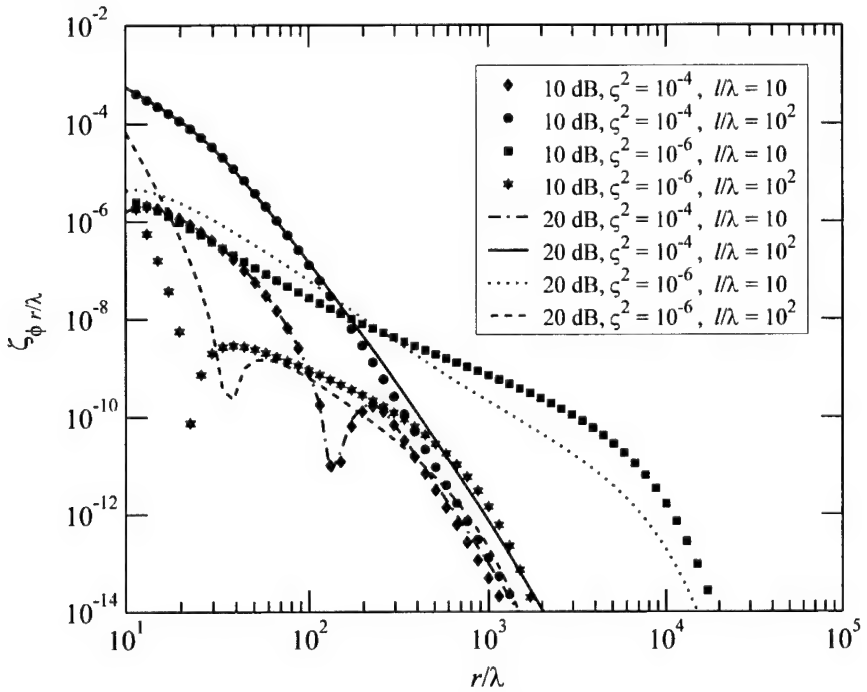

Figure 12. Coupling between ϕ and r/λ as a function of normalized propagation distance. Parameters same as figure 9. (Analogous plots for $\zeta_{\theta,\,r/\lambda}$ have same behavior and almost same values.)

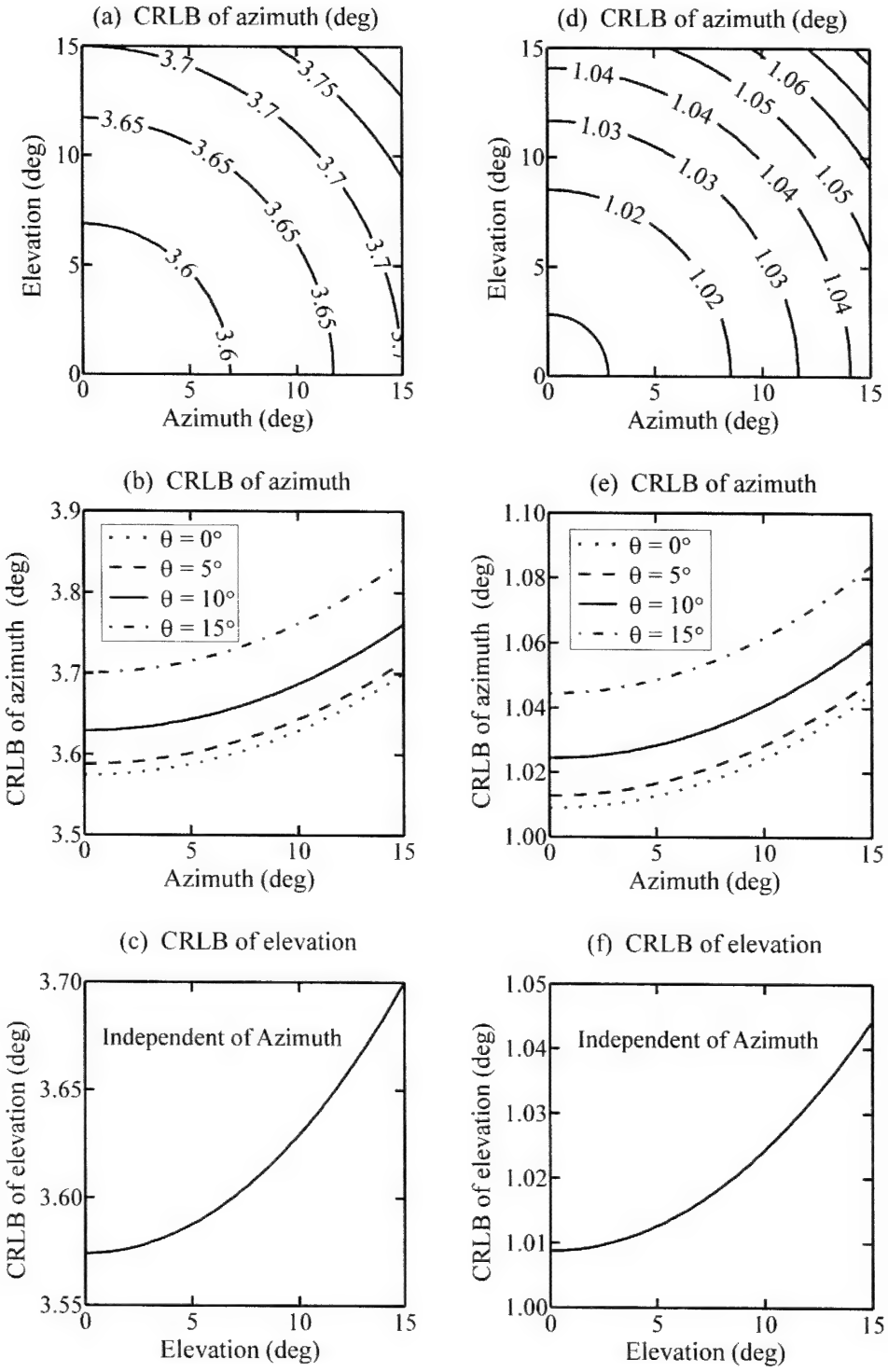

Figure 13. Angular dependence of σ_ϕ and σ_θ. In (a–c): $\varsigma^2 = 10^{-4}$, $\ell/\lambda = 10$, $r/\lambda = 500$, $\mathrm{SNR}_0 = 10$ dB at $\mathcal{R}/\lambda = 500$, and scalar von Kármán spectrum. Same in (d–f), but $\varsigma^2 = 10^{-6}$.

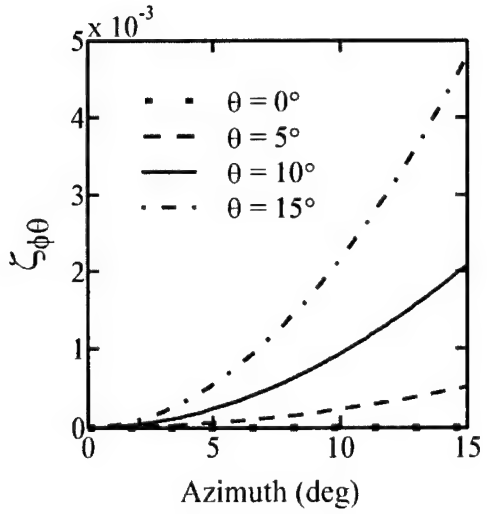

Figure 14. Coupling between ϕ and θ. Results valid for both spectra and all values of ς^2, ℓ/λ, and SNR_0 when $r/\lambda \gtrapprox 100$.

5.2 CRLBs of Other Parameters

For the PW case, it was found [2] that there was not sufficient information to provide reasonable estimates of the propagation distance and turbulence parameters. For the spherical-wave model, we again find that we cannot estimate r/λ, ς^2, ℓ/λ, or SNR_0. Even when ς^2, ℓ/λ, and SNR_0 are not considered as unknowns, r/λ cannot be estimated.

As the turbulence parameters cannot be estimated from this model, it follows that they must be calculated from models that consider meteorological data. There are models based on von Kármán's spectrum that calculate the turbulence parameters in the energy-containing subrange of the turbulence [9,10]. These models consider contributions to the sound speed variations from wind and temperature fluctuations produced by both shear and buoyancy instabilities.

6. Conclusions

We have investigated the Cramer-Rao lower bounds of the wave-front angles of arrival for a spherical wave propagating through atmospheric turbulence with fluctuation described by a von Kármán spectrum. This investigation is the logical continuation of previous investigations [1,2] for a plane wave source. Both investigations consider a deterministic mean, two bearing angles, and multiple unknown parameters. The use of a spherical-wave model reduces the CRLBs of the AOAs from those of the plane-wave model due to the change in the mutual coherence function. The coupling of the estimates of the angles of arrival to the estimates of the normalized propagation distance and source phase are found to be minimal, if not completely negligible. And the estimates of the angles of arrival are decoupled from the estimates of the turbulence parameters and signal-to-noise ratio. The coupling between the two bearing angles is the same as for the plane-wave model when the normalized propagation distance is consistent with the parabolic approximation.

As the estimation of the turbulence parameters does not effect the estimates of the AOAs, it is logical to extend the calculation of the mutual coherence function to include contributions from both scalar and vector spectra. Such a model is considered in Ref. [13], in which the MCF is calculated from meteorological data.

The significance of scattering by atmospheric turbulence is evident from the results presented here. In order to understand and circumvent limitations on U. S. Army acoustical tracking systems, it is necessary to predict the performance of acoustic sensor arrays for various atmospheric conditions. This analysis clearly demonstrates the atmospheric conditions that are unfavorable for accurate acoustical tracking.

This investigation is limited by the model of the second moment for oblique incidence, as well as the fact that other physical phenomena, such as ground reflections and refraction by atmospheric wind and temperature gradients, which have not been included in this analysis, may have a considerable impact on the ability to estimate the elevation.

Acknowledgments

The authors are grateful to V. E. Ostashev of NOAA/Environmental Technology Laboratory for many helpful discussions.

Appendix A. Nomenclature

A.1 Symbols

$\mathbb{C}$	Complex
$*$	Complex conjugate
$\equiv$	Defined as
$\in$	Element of
$\langle\cdot\rangle$	Ensemble average or expectation value
$\dagger$	Hermitian adjoint (complex conjugate transpose)
$\mathbf{I}_n$	Identity matrix, $n \times n$
$\Im$	Imaginary
$\sim$	On the order of
$\Re$	Real
T	Transpose

A.2 Acronyms

AOA	Angle of arrival
AOB	Angle of bearing
CRLB	Cramer-Rao lower bound
FI	Fisher information
LOS	Line of sight
MCF	Mutual coherence function
MLE	Maximum likelihood estimator
MSE	Mean-square error
PDF	Probability density function
PW	Plane wave
SAA	Small angle approximation
SNR	Signal-to-noise ratio

SW	Spherical wave
2D	Two dimensions or two-dimensional
3D	Three dimensions or three-dimensional

References

1. S. L. Collier and D. K. Wilson, " Performance Bounds on Atmospheric Acoustic Sensor Arrays Operating in a Turbulent Medium I. Plane-Wave Analysis," U. S. Army Research Laboratory Technical Report, Adelphi, MD, ARL-TR-2426 (February 2002).

2. S. L. Collier and D. K. Wilson, " Performance bounds for passive sensor arrays operating in a turbulent medium: Plane-wave analysis," submitted to J. Acoust. Soc. Am.

3. D. K. Wilson, "Performance bounds for acoustic direction-of-arrival arrays operating in atmospheric turbulence," J. Acoust. Soc. Am. **103**, 1306–1319 (1998).

4. B.-G. Song and J. A. Ritcey, "Angle of arrival estimation of plane waves propagating in random media," J. Acoust. Soc. Am. **99**, 1370–1379 (1996).

5. V. E. Ostashev, *Acoustics in Moving Inhomogeneous Media* (E & FN Spon, London, 1997).

6. A. Ishimaru, *Wave Propagation and Scattering in Random Media* (IEEE Press, Piscataway, NJ, 1997).

7. S. M. Rytov, Yu. A. Kravtsov, and V. I. Tatarskii, *Principles of Statistical Radiophysics 4: Wave Propagation Through Random Media* (Springer-Verlag, New York, 1989).

8. S. M. Flatté, editor, *Sound Transmission Through a Fluctuating Ocean,* (Cambridge University Press, Cambridge, 1979).

9. V. E. Ostashev and D. K. Wilson, "Relative Contributions from Temperature and Wind Velocity Fluctuations to the Statistical Moments of a Sound Field in a Turbulent Atmosphere," Acustica **86**, 260–268 (2000).

10. D. K. Wilson, "A turbulence spectral model for sound propagation in the atmosphere that incorporates shear and buoyancy forcings," J. Acoust. Soc. Am. **108**, 2021–2038 (2000).

11. S. M. Kay, *Fundamentals of Statistical Signal Processing: Estimation Theory* (PTR Prentice Hall, Englewood Cliffs, NJ, 1993).

12. S. L. Collier and D. K. Wilson, "Cramer-Rao Lower Bounds of Angle-of-Arrival Estimates for Acoustic Sensor Arrays Operating in Atmospheric Turbulence," *Proceedings of the 2001 Meeting of the MSS Specialty Group on Battlefield Acoustic and Seismic Sensing, Magnetic and Electric Field Sensors, Vol. II, Held 24–26 October 2001, Applied Physics Lab/Johns Hopkins University, Laurel, MD.* (Infrared Information Analysis Center, 2002).

13. S. L. Collier and D. K. Wilson, "Passive Acoustic Localization in Atmospheric Turbulence: Experiment and Theory," *Proceedings of the 22nd Army Science Conference, 11–13 December 2000, Renaissance Harborplace Hotel, Baltimore, MD.*

REPORT DOCUMENTATION PAGE

Form Approved
OMB No. 0704-0188

1. AGENCY USE ONLY *(Leave blank)*	2. REPORT DATE	3. REPORT TYPE AND DATES COVERED
	February 2003	Final, 01/01-08/02

4. TITLE AND SUBTITLE
Performance Bounds on Atmospheric Acoustic Sensor Arrays Operating in a Turbulent Medium II. Spherical-Wave Analysis

5. FUNDING NUMBERS
DA PR: B53A
PE: 61102A

6. AUTHOR(S)
Sandra L. Collier and D. Keith Wilson

7. PERFORMING ORGANIZATION NAME(S) AND ADDRESS(ES)
U.S. Army Research Laboratory
Attn: AMSRL- CI-EE

8. PERFORMING ORGANIZATION REPORT NUMBER
ARL-TR-2904

9. SPONSORING/MONITORING AGENCY NAME(S) AND ADDRESS(ES)
U.S. Army Research Laboratory
2800 Powder Mill Road
Adelphi, MD 20783-1197

10. SPONSORING/MONITORING AGENCY REPORT NUMBER

11. SUPPLEMENTARY NOTES
ARL PR: 3FEJ26
AMS code: 61110253A11

12a. DISTRIBUTION/AVAILABILITY STATEMENT
Approved for public release; distribution unlimited.

12b. DISTRIBUTION CODE

13. ABSTRACT *(Maximum 200 words)*
The performance bounds of a passive acoustic array operating in a turbulent medium with fluctuations described by a von Kàrmàn spectrum are investigated. This treatment considers a single, monochromatic, spherical-wave source and a line-of-sight propagation path. The Cramer-Rao lower bounds of the wave-front angles of arrival are calculated for an unknown parameter set which includes the propagation distance, turbulence parameters, source phase, and signal-to-noise ratio.

14. SUBJECT TERMS
Angle of arrival, Cramer-Rao lower bound, Fisher information, atmospheric turbulence, random medium.

15. NUMBER OF PAGES
37

16. PRICE CODE

17. SECURITY CLASSIFICATION OF REPORT	18. SECURITY CLASSIFICATION OF THIS PAGE	19. SECURITY CLASSIFICATION OF ABSTRACT	20. LIMITATION OF ABSTRACT
Unclassified	Unclassified	Unclassified	SAR